Jadavpur University

Department of Physics

Space-Time Distributions of Electro-Magnetic Fields in Relativistic Nuclear Collisions

Shashank Jaiswal

Supervisor: Prof. Mitali Mondal

A report submitted in partial fulfillment of the requirements of
the Jadavpur University for the degree of
Master of Science in *Physics*

July 9, 2025

Declaration

I, Shashank Jaiswal, of the Department of Physics, Jadavpur University, confirm that this is my own work and figures, tables, equations, code snippets, artworks, and illustrations in this report are original and have not been taken from any other person's work, except where the works of others have been explicitly acknowledged, quoted, and referenced. I understand that if failing to do so will be considered a case of plagiarism. Plagiarism is a form of academic misconduct and will be penalized accordingly.

I give consent to a copy of my report being shared with future students as an exemplar.

I give consent for my work to be made available more widely to members of UoR and public with interest in teaching, learning and research.

Shashank Jaiswal
July 11, 2025

Abstract

In this thesis, we investigate the event-by-event generation of electromagnetic fields in ultra-relativistic heavy-ion collisions using the Monte Carlo Glauber model. The study is focused on Pb–Pb collisions, where nucleons are spatially distributed according to the Woods–Saxon nuclear density profile. By simulating individual collision events, we incorporate essential features of the Glauber framework such as participant and spectator nucleon distinction, binary nucleon–nucleon collisions, and impact parameter dependence.

A detailed implementation of the Monte Carlo Glauber approach is presented, highlighting the computation of initial geometric quantities like the number of participant nucleons (N_{part}), the number of binary collisions (N_{coll}), and participant-plane eccentricities (ε_n). These quantities are then used as input for calculating the space–time evolution of electromagnetic fields generated during collisions. The Liénard–Wiechert potentials are employed in the relativistic limit to evaluate electric and magnetic field components arising from both participant and spectator charges.

This work provides a computational framework and physical insight into the interplay between collision geometry and electromagnetic field generation, which is crucial for understanding various signatures in high-energy heavy-ion experiments.

Acknowledgements

I take this opportunity to express my sincere gratitude to all those who have contributed to the successful completion of this dissertation.

First and foremost, I am deeply indebted to my supervisor, **Prof. Mitali Mondal**, for her invaluable guidance, unwavering support, and insightful suggestions throughout the course of this work. Her mentorship, encouragement, and patience have been instrumental in shaping this research, and I am truly grateful for her continuous involvement at every stage.

I would also like to extend my heartfelt regards to my joint supervisor for my project **Dr. Subikash Choudhury**, Postdoctoral Researcher in High Energy Physics, for his expert advice and constructive inputs regarding the simulation of Heavy-Ion Collisions at relativistic energies. His perspectives significantly enriched the technical foundation of this project.

Furthermore, I am grateful to my fellow classmates and all my professors for their camaraderie and for sharing ideas that meaningfully contributed to the overall quality of this work. Their collaboration and discussions provided both motivation and clarity throughout the research process.

This acknowledgement reflects a collective effort, and I am sincerely thankful to all who supported and inspired me during this academic journey.

Shashank Jaiswal
Final Year, M.Sc. in Physics
Examination Roll No.: PPHYE0256032
Registration No.: 165447

Contents

List of Figures

List of Tables

List of Abbreviations

LHC	Large Hadron Collider
RHIC	Relativistic Heavy Ion Collider
MC	Monte Carlo
QGP	Quark-Gluon Plasma
QCD	Quantum Chromodynamics
CM	Centre of Mass
ZDC	Zero Degree Calorimeter
HIJING	Heavy Ion Jet Interaction Generator

Chapter 1

Introduction

High-energy heavy-ion collisions offer a unique window into the properties of nuclear matter under extreme conditions, particularly the formation of the quark-gluon plasma (QGP)—a deconfined state of quarks and gluons thought to have existed in the early universe. This thesis focuses on collisions of lead (Pb) nuclei at relativistic velocities, emphasizing the electromagnetic field distributions generated in such events using the Monte Carlo (MC) Glauber model.

The foundation of Glauber modeling lies in its statistical description of collision geometry, based on nucleon positions sampled from nuclear density distributions, typically the Woods-Saxon profile. In its Monte Carlo implementation, each event is modeled by randomly drawing nucleon coordinates, computing participant nucleons (N_{part}) and binary collisions, and deriving geometric quantities such as impact parameter and eccentricities (elliptical ε_2 and triangular ε_3) Wang et al. (2024, 2021).

Ray and Daugherity (2008) critically evaluated the MC Glauber model across multiple collision systems. They demonstrated that central collision observables—impact parameter, N_{part}, number of binary interactions (N_{bin}), and collision frequency (ν)—could be constrained with reduced uncertainties when model parameters are calibrated against mid-rapidity multiplicity distributions Glauber et al. (2008).

Earlier work by Cugnon *et al.* (1980) developed Monte Carlo simulations based on cascade models, where nucleon–nucleon interactions are treated as independent binary collisions, including resonance production and decays. Their approach yielded reasonable agreement with proton and pion yields in intermediate-energy nucleus–nucleus collisions Cugnon (1980), laying groundwork for subsequent Glauber-based geometry descriptions.

More recent studies, such as Wang *et al.* (2021), applied MC Glauber simulations to ultra-relativistic Pb–Pb collisions at $\sqrt{s_{\text{NN}}} = 5.5$ TeV. Their work revisited event eccentricities ε_2 and ε_3, confirming an inverse relationship between eccentricity values and N_{part}, with peripheral events (40–50% centrality) exhibiting $\varepsilon_2 \approx 0.4$–$0.5$ and $\varepsilon_3 \approx 0.3$. In particular, the $\varepsilon_3/\varepsilon_2$ ratio increases from approximately 0.5 in central collisions to nearly unity in more peripheral cases, underlining the importance of triangular flow in understanding initial-state geometry fluctuations Wang et al. (2021).

Together, these studies establish the MC Glauber model as an essential framework for:

- Simulating spatial configurations of nucleons in colliding nuclei
- Quantifying centrality-dependent geometric parameters
- Investigating the interplay of eccentricities (ε_2 and ε_3) with hydrodynamic flow observables

- Providing a basis for computing initial electromagnetic fields stemming from collision geometry

In this thesis, we extend these approaches to evaluate electromagnetic fields generated in Pb–Pb collisions at relativistic energies. By implementing a Glauber-based simulation of nucleon distributions and collision dynamics, we calculate the space–time evolution of electromagnetic fields and correlate these fields with collision geometry metrics such as N_{part}, eccentricities, and impact parameter. This enables deeper insight into electromagnetic phenomena accompanying QGP formation and evolution.

1.1 Physics of High-energy Heavy-ion Collisions :

High-energy heavy-ion collisions are an interdisciplinary field which connects the high-energy physics of elementary particles with nuclear physics. There exist also connections to astrophysics & cosmology.

These are relativistic-energy collisions, where the kinetic energy exceeds the rest energy significantly. The name 'heavy-ions' is used for heavy atomic nuclei like Pb(208) or Au(197) etc..

In high-energy heavy-ion collisions, very large numbers of particles are produced (large **multiplicities**). For example, in the central Au+Au collisions at RHIC (Relativistic Heavy-Ion Collider - Brookhaven National Laboratory), at the highest beam energy $\sqrt{S_{NN}} = 200$ GeV, the total charged particle multiplicity is about 5000. Hence, the number of particles produced exceeds the number of initial nucleons by a factor of 10.

In this situation, different theoretical methods are used, which are suitable for description of large macroscopic systems, e.g., Thermodynamics, Hydrodynamics, Kinetic (Transport) theory, Field Theory at finite temperature & density, Non-equilibrium Field Theory, Monte Carlo simulations.

The high-energy nuclear collision is a system of many-body strongly interacting particles The fundamental theory of the strong interactions is Quantum Chromodynamics (QCD), the theory of Quarks & Gluons which are confined in hadrons, i.e., Baryons (Which are Fermions) & Mesons (Which are Bosons).

1.2 Necessity of High-energy Collision

High-energy heavy-ion collisions are essential tools in modern nuclear and particle physics, particularly for probing the properties of strongly interacting matter under extreme conditions. The motivations for studying such collisions include the following:

1. **Creation of Quark–Gluon Plasma (QGP):**
   At sufficiently high energy densities and temperatures (exceeding the QCD critical temperature $T_c \sim 150$ MeV), nuclear matter undergoes a phase transition from hadronic matter to a deconfined state of quarks and gluons known as the quark–gluon plasma (QGP). High-energy collisions provide the conditions necessary to create and study this exotic state of matter Heinz and Jacob (2000); B. Muller and Wyslouch (2012).

2. **Access to Early Universe Conditions:**
   The energy densities and temperatures achieved in these collisions are similar to those present microseconds after the Big Bang. Thus, heavy-ion collisions act as a 'microlaboratory' to investigate early universe physics B. Muller and Wyslouch (2012).

3. **Study of Collective Behavior and Fluid Dynamics:**
   The produced QGP behaves like an almost perfect fluid with minimal shear viscosity. High-energy collisions allow us to study relativistic hydrodynamic expansion and phenomena such as anisotropic flow, vorticity, and particle correlations D. Teaney and Shuryak (2001); Song and Heinz (2011).

4. **Electromagnetic and Anomalous Phenomena:**
   Ultra-relativistic velocities lead to the generation of extremely strong electromagnetic fields ($\sim 10^{15}$–10^{16} T), enabling the exploration of phenomena such as the chiral magnetic effect and magnetic helicity Deng and Huang (2012); D. E. Kharzeev (2016).

5. **Testing Quantum Chromodynamics (QCD) in Extreme Regimes:**
   High-energy nuclear collisions provide a unique testing ground for non-perturbative aspects of QCD, including parton saturation, color-glass condensate, and hadronization mechanisms Gelis (2013).

6. **Study of Phase Transitions and Critical Behavior:**
   By varying the collision energy and the size of the system, experiments can map the QCD phase diagram and search for a critical point or signatures of phase coexistence Stephanov (2004).

7. **Benchmarking Theoretical Models:**
   High-energy data serve to constrain and validate models such as the Glauber model, transport codes, hydrodynamics, and jet energy-loss formalisms. These are crucial for developing a consistent theoretical picture of heavy-ion dynamics Miller et al. (2007*b*).

1.3 Necessity of Simulating the Collisions

High-energy heavy-ion collisions offer a unique window into the properties of nuclear matter under extreme conditions, particularly the formation of the quark–gluon plasma (QGP)—a deconfined state of quarks and gluons thought to have existed in the early universe. This thesis focuses on collisions of lead (Pb) nuclei at relativistic velocities, emphasizing the electromagnetic field distributions generated in such events using the Monte Carlo (MC) Glauber model.

The foundation of Glauber modeling lies in its statistical description of collision geometry, based on nucleon positions sampled from nuclear density distributions—typically the Woods–Saxon profile. In its Monte Carlo implementation, each event is modeled by randomly drawing nucleon coordinates, computing participant nucleons (N_{part}) and binary collisions (N_{bin}), and deriving geometric quantities such as impact parameter and eccentricities (elliptical ε_2 and triangular ε_3) Loizides et al. (2018); Hirano and Nara (2013).

Ray and Daugherity (2008) critically evaluated the MC Glauber model across various collision systems, showing that central collision observables—impact parameter, N_{part}, N_{bin}, and collision frequency (ν)—could be constrained with reduced uncertainties when model parameters are tuned to mid-rapidity multiplicity distributions Glauber et al. (2008). Earlier work by Cugnon *et al.* (1980) employed Monte Carlo cascade models of nucleon–nucleon interactions, including resonance production, and found good agreement with proton and pion yields in intermediate-energy collisions Cugnon (1980).

More recent studies, such as Wang *etal.* (2021), applied MC Glauber simulations to ultra-relativistic Pb–Pb collisions at $\sqrt{s_{\text{NN}}} = 5.5$TeV, finding that eccentricities ε_2 and ε_3 inversely correlate with N_{part}, and that the $\varepsilon_3/\varepsilon_2$ ratio rises from 0.5 to near unity toward

peripheral collisions Wang et al. (2021). Loizides *etal.* (2018, erratum 2019) further refined Glauber modeling by incorporating separate neutron–proton density profiles, nodal separation, and recentering procedures. These improvements led to up to 7% changes in central values of Glauber quantities, but generally reduced systematic uncertainties below 5% across centralities and energies Loizides et al. (2018, 2019).

Integrated dynamical models combining Glauber initial conditions with viscous hydrodynamics have been successful in describing a wide array of flow observables at RHIC and LHC energies Hirano and Nara (2013). However, challenges remain—such as the "ultra-central flow puzzle," where hydrodynamic models overestimate the ratio $v_2\{2\}/v_3\{2\}$ compared to experimental data in ultra-central Pb–Pb collisions—highlighting the importance of precise initial-state modeling Hirano and Nara (2013). Additionally, measurement-driven improvements in Glauber inputs, such as neutron-skin corrections and density fluctuations, have enhanced the predictive power of models for collision geometry Loizides et al. (2018).

Motivation for Simulation Simulating high-energy heavy-ion collisions using MC Glauber and dynamical models is essential because it:

- Generates realistic initial geometries and participant distributions for collisions at various energies and impact parameters.
- Enables correlations between collision geometry (e.g., eccentricities, N_{part}) and final-state observables, such as collective flow and particle yields.
- Supports calculation of initial electromagnetic fields, which are critical in phenomena like the chiral magnetic effect and photon production.
- Helps probe QGP properties (e.g., viscosities, equation of state) through comparison of simulated flow observables and experimental data.
- Reduces uncertainties in geometry-based quantities, enabling more accurate interpretation of heavy-ion measurements.

In this thesis, we harness improved Monte Carlo Glauber simulations of Pb–Pb collisions to compute the space–time evolution of electromagnetic fields and explore their correlations with key collision geometry metrics like N_{part}, ε_2, ε_3, and impact parameter. This approach aims to shed light on the electromagnetic signatures accompanying QGP formation and evolution.

1.4 Fundamental Concepts of Heavy-ion Interaction :

At very high energies, simple geometric concepts are often used.

1.4.1 Participants & Spectators :

Within the Glauber model framework, nucleons in colliding nuclei are classified into two categories based on their interactions during the collision:

- **Participants**(N_{part}) **:**
  These are nucleons that undergo at least one inelastic collision with a nucleon from the other nucleus. Participants contribute directly to the production of secondary particles and define the geometry of the interaction zone *Participants and spectators at the heavy-ion fireball* (2012); et al. (2007).

- **Spectators**(N_{spec}) **:**
  These are nucleons that do *not* partake in any inelastic collision. They continue traveling along their initial beam trajectory, largely unaffected by the collision dynamics *Participants and spectators at the heavy-ion fireball* (2012); et al. (2014).

Key Features

1. The number of participants, N_{part}, and the number of spectators, N_{spec}, satisfy:

$$N_{\text{spec}} = 2A - N_{\text{part}},$$

   where A is the mass number of each nucleus in a symmetric collision *Participants and spectators at the heavy-ion fireball* (2012).

2. Participants define the "overlap zone" responsible for particle production, while spectators are detected in forward regions and serve as indicators of collision centrality via Zero Degree Calorimeters (ZDCs) *Participants and spectators at the heavy-ion fireball* (2012); Segal and Taranenko (2023).

1.4.2 Impact Vector (b) & Impact Parameter (B) :

In relativistic heavy-ion collisions, two key geometric quantities are used to characterize the collision geometry:

- **Impact Parameter (B):** The impact parameter is defined as the transverse distance between the centers of the two colliding nuclei. It determines the collision centrality: smaller values of B correspond to central collisions, while larger b values correspond to more peripheral or ultraperipheral collisions *Lectures on high-energy heavy-ion collisions at the LHC* (2009); Miller et al. (2007*a*). Mathematically, it is given by:

$$B = |\mathbf{b}|,$$

  where $\mathbf{b}$ is the impact vector in the transverse plane.

- **Impact Vector (b):** The impact vector is a two-dimensional vector in the transverse plane that points from the center of the target nucleus to the center of the projectile nucleus. Its magnitude equals the impact parameter, and its direction defines the reaction plane in each collision event Anonymous (2020).

1.4.3 Number of Binary Collisions (N_{coll}) :

In the Glauber model framework, the total number of binary collisions between nucleons from the two colliding nuclei is defined as:

$$N_{\text{coll}}(b) = \sum_{i \in A} \sum_{j \in B} P_{ij}(b),$$

where $P_{ij}(b)$ is the probability of an inelastic collision between nucleon i in nucleus A and nucleon j in nucleus B at impact parameter b.

1.4.4 Number of Hard-Collisions (N_{hard}) :

In the context of high-energy heavy-ion collisions, **hard collisions** refer to rare, large-momentum-transfer (high-p_T) parton–parton scatterings, such as those leading to jets, heavy quarks, or electroweak bosons. In the Glauber formalism, these processes are assumed to scale with the number of binary nucleon–nucleon collisions, N_{coll} d'Enterria (2003).

The yield of a hard process in nucleus–nucleus (A+B) reactions at a given impact parameter b is thus estimated by:

$$Y^{AB}_{\text{hard}}(b) = N_{\text{coll}}(b)\,\sigma^{NN}_{\text{hard}},$$

where $\sigma^{NN}_{\text{hard}}$ is the corresponding cross-section in nucleon–nucleon collisions (pp) at the same energy d'Enterria (2003).

1.4.5 Participant-plane Eccentricity (ϵ_2) & Momentum Anisotropy (v_2) :

In relativistic heavy-ion collisions, **eccentricity** is a geometrical measure of the anisotropy of the overlapping region formed by the two colliding nuclei in the transverse plane (perpendicular to the beam direction). It quantifies how much the shape of the initial matter distribution deviates from circular symmetry and is directly linked to the azimuthal asymmetries observed in the final-state particle momentum distributions.

Standard Eccentricity (ε_{std}): In a smooth, event-averaged picture, the standard (or reaction-plane) eccentricity is defined as:

$$\varepsilon_{\text{std}} = \frac{\sigma_y^2 - \sigma_x^2}{\sigma_y^2 + \sigma_x^2},$$

where σ_x^2 and σ_y^2 are the variances of the nucleon distribution in the x and y directions respectively, with the x-axis defined along the impact parameter vector (reaction plane).

Participant Eccentricity ($\varepsilon_{\text{part}}$): In individual events, due to fluctuations in the positions of participating nucleons, the initial shape of the matter distribution may be tilted with respect to the reaction plane. To account for this, the participant-plane eccentricity is introduced:

$$\varepsilon_{\text{part}} = \frac{\sqrt{(\sigma_y^2 - \sigma_x^2)^2 + 4\sigma_{xy}^2}}{\sigma_y^2 + \sigma_x^2},$$

where σ_{xy} is the covariance of the x and y distributions. This quantity better reflects the true anisotropy seen by the hydrodynamic evolution of the system and is used in event-by-event simulations.

Physical Significance: Eccentricity acts as the driving force behind anisotropic flow phenomena, especially the second Fourier coefficient v_2 (elliptic flow). A higher initial eccentricity leads to stronger pressure gradients, which in turn produce greater anisotropy in the momentum distribution of the emitted particles Miller et al. (2007*b*); D. Teaney and Shuryak (2001).

Applications: The study of eccentricity fluctuations is crucial for understanding:

- Centrality dependence of elliptic flow.
- Event-plane correlations.

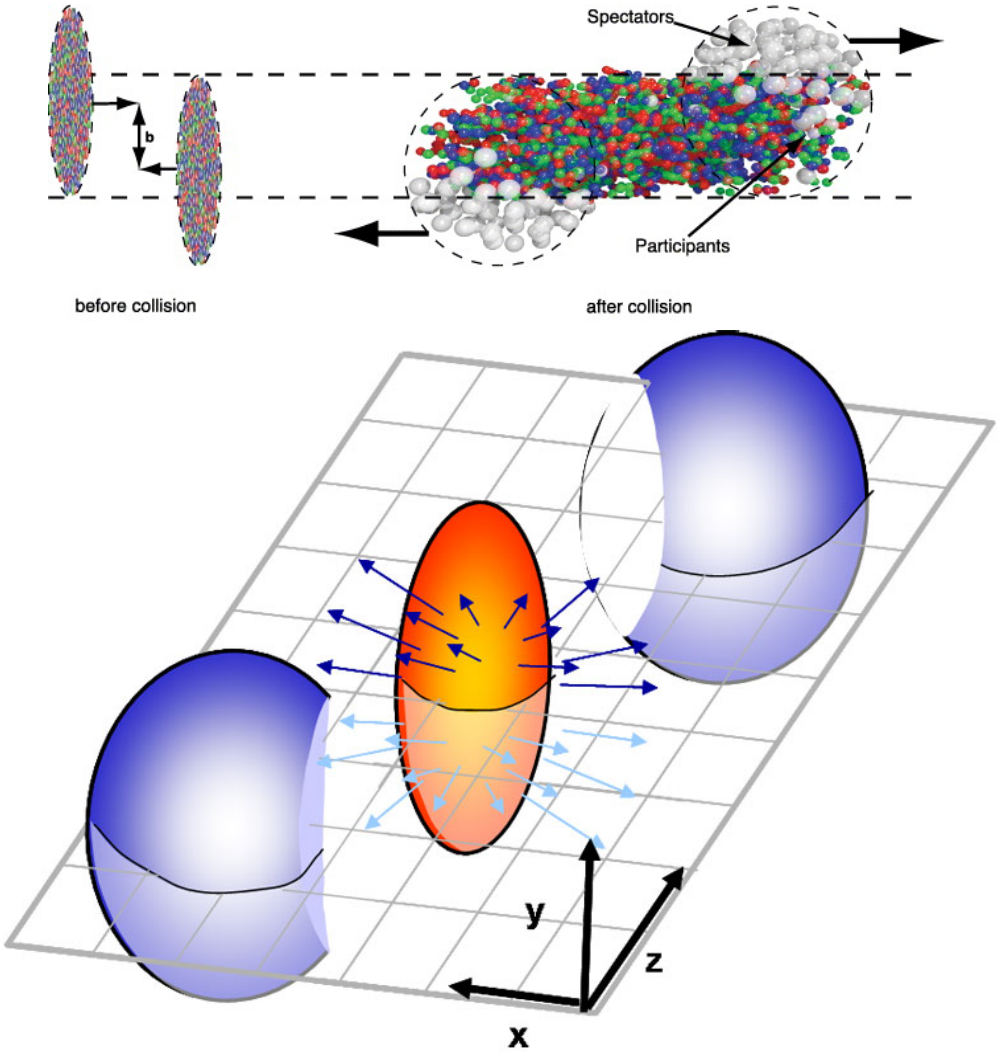

Figure 1.1: Schematic representation of Optical Glauber model geometry. Tejeda-Yeomans (2020); Esha (2012)

- Initial-state geometry modeling for hydrodynamics.
- Jet quenching path-length dependence.

For non- central collisions, the shape of the interaction region depends strongly on the impact parameter of the collision. Just after a non-central collision, the reaction volume is an ellipsoidal. This spatial anisotropy is translated into the momentum anisotropy of the produced particles.

Momentum anisotropy refers to the azimuthal (angular) asymmetry in the distribution of final-state particle momenta in the transverse plane, which arises due to the pressure gradients generated by the initial spatial anisotropy of the nuclear overlap region.

In non-central heavy-ion collisions, the initial overlap region is typically elliptical. This spatial eccentricity leads to different pressure gradients along different directions in the transverse plane, resulting in more particles being emitted along the short axis than the long axis. This anisotropic collective expansion is quantified by the Fourier coefficients of the azimuthal distribution of produced particles.

Fourier Decomposition: The azimuthal dependence of the particle yield can be expanded as:

$$\frac{dN}{d\phi} = \frac{N}{2\pi}\left(1 + 2\sum_{n=1}^{\infty} v_n \cos[n(\phi - \Psi_n)]\right),$$

where:

- ϕ is the azimuthal angle of the emitted particle,
- v_n are the Fourier coefficients,
- Ψ_n is the n^{th}-order event plane angle.

The second-order coefficient v_2, known as **elliptic flow**, is the most prominent and widely studied observable of momentum anisotropy:

$$v_2 = \langle \cos[2(\phi - \Psi_2)] \rangle.$$

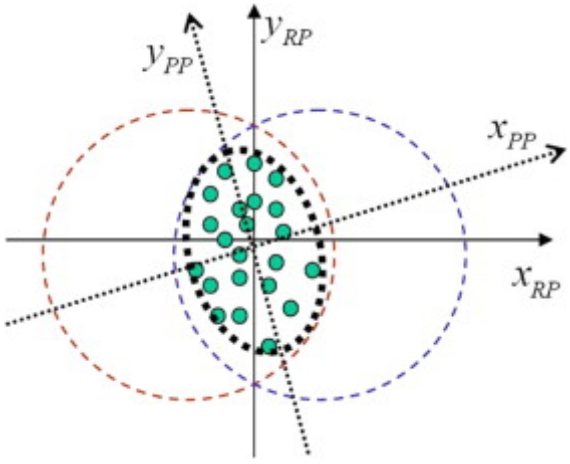

Figure 1.2: Reaction plane and participant plane Esha (2012)

Physical Significance:

- Momentum anisotropy reflects the collective behavior of the quark–gluon plasma.
- It provides information about the transport properties (e.g., viscosity) of the medium.
- Event-by-event fluctuations in momentum anisotropy help constrain initial condition models and the response of the system to geometry.

In the upcoming chapters we are going to understand the step-by-step introduction and formulation for the project. The next chapter presents the theoretical background necessary to understand relativistic heavy-ion collisions and the role of electromagnetic fields in such events. Chapter 3 introduces the Glauber model and discusses its fundamental structure and assumptions. Chapter 4 describes the Monte Carlo approach to the Glauber model, detailing the event-by-event simulation process. Chapter 5 explains the conclusion of the observations and outputs and frames the possible future works using the outputs.

Chapter 2

The Glauber Model

2.1 Introduction :

The Glauber model serves as a cornerstone for understanding and quantifying the geometry of relativistic heavy-ion collisions. Originally introduced to describe multiple scattering processes in quantum mechanics, its modern application adapts this framework into a predominantly geometric picture suitable for interpreting experimental data in high-energy nuclear physics Miller et al. (2007*b*,*a*).

Within this model, key geometric observables—such as the impact parameter (b), number of participating nucleons (N_{part}), and number of binary nucleon–nucleon collisions (N_{coll})—are calculated based on the spatial overlap of the colliding nuclei. These quantities underpin the classification of collision centrality and facilitate a systematic comparison of experimental measurements across different collision systems and energies Miller et al. (2007*a*).

The robust application of Glauber modeling is further evidenced by its widespread use among major collider experiments (such as those at RHIC), where it consistently provides similar estimates for geometric quantities despite variations in implementation methods Miller et al. (2007*b*). Moreover, the reliability of these estimates has made them integral to interpreting a range of experimental observables—including charged-particle multiplicities, anisotropic flow coefficients, jet quenching signatures, and rare probes like quarkonia suppression—all of which exhibit clear dependence on the underlying collision geometry Miller et al. (2007*a*).

In this thesis, the Glauber model will form the geometric backbone informing our Monte Carlo simulations of Pb–Pb collisions. By determining b, N_{part}, and N_{coll} event by event, we establish a foundational geometric framework upon which we base subsequent calculations of electromagnetic field distributions and their relation to collision dynamics.

2.2 Assumptions :

The Glauber model, as applied to high-energy nuclear collisions, relies on a set of fundamental assumptions that simplify the complex dynamics of interacting nucleons into a tractable, geometry-based framework. These assumptions provide the basis for calculating quantities such as the number of participant nucleons (N_{part}), the number of binary collisions (N_{coll}), and the impact parameter (b). The main assumptions are as follows Miller et al. (2007*b*,*a*):

1. **Straight-line Trajectories:**
   Nucleons from each nucleus travel along straight-line paths in the beam direction during the collision. This eikonal approximation is valid due to the high Lorentz boost of the colliding nuclei, which minimizes deflection over the short collision timescale.

2. **Instantaneous Interaction:**
   The nucleon–nucleon interactions are assumed to occur instantaneously at the point of closest approach, with no time evolution of the internal nucleon structure considered.

3. **Independent Binary Collisions:**
   Each nucleon–nucleon collision is treated as independent of others, without accounting for coherence effects or final-state interactions among products of multiple collisions.

4. **Frozen Nucleon Configuration:**
   The positions of the nucleons within each nucleus are "frozen" during the collision. The spatial configuration of nucleons is sampled from a probability distribution (typically a Woods–Saxon form), and this configuration remains fixed for the duration of the event.

While these assumptions introduce simplifications, they remain well justified for ultra-relativistic collisions where the geometrical configuration and global event characteristics dominate the early stages of the reaction. These assumptions also make the Glauber model particularly suitable as an initial-state generator for more detailed dynamical models such as hydrodynamics or transport simulations.

2.3 Variants :

The Glauber model can be studied in two variants:

1. The Optical Approach

2. The Monte Carlo Approach

2.3.1 Optical Approach :

The optical Glauber model is a continuous, analytic approximation of the Monte Carlo Glauber method, where nuclear density profiles are treated as smooth matter distributions rather than discrete collections of individual nucleons. Instead of simulating event-by-event nucleon positions, the optical model computes average quantities by integrating over the nuclear density functions.

In this approach, the nuclei are described by continuous nucleon density functions $\rho_A(\tilde{r})$ and $\rho_B(\tilde{r})$, typically parameterized by a Woods–Saxon distribution. The thickness function $T_A(\tilde{s})$ is defined as the integral of the density along the beam axis:

$$T_A(\tilde{s}) = \int dz\, \rho_A(\tilde{s}, z), \tag{2.1}$$

where $\tilde{s}$ is the transverse coordinate in the collision plane. The probability of interaction between the two nuclei is then expressed in terms of these thickness functions.

The total number of binary nucleon–nucleon collisions is computed as:

$$N_{\text{coll}}(b) = \sigma_{NN}^{\text{inel}} \int d^2s\, T_A(\tilde{s})\, T_B(\tilde{s} - \tilde{b}), \tag{2.2}$$

and the number of participating nucleons is given by:

$$N_{\text{part}}(b) = \int d^2s \left[T_A(\tilde{s}) \left(1 - \left[1 - \frac{\sigma_{NN}^{\text{inel}}\, T_B(\tilde{s} - \tilde{b})}{B} \right]^B \right) + (A \leftrightarrow B) \right], \tag{2.3}$$

where A and B are the mass numbers of the two nuclei and b is the impact parameter.

The optical model is computationally efficient and provides smooth estimates of geometric quantities such as N_{part}, N_{coll}, and eccentricities. However, it does not account for event-by-event fluctuations and correlations between nucleons, making it less suited for observables that are sensitive to such fluctuations.

While the Optical Glauber model offers a useful baseline and fast computation, modern studies increasingly favor the Monte Carlo implementation for more accurate and fluctuation-sensitive analysis—especially in small systems or in the study of flow harmonics.

2.3.2 Monte Carlo Approach :

The Monte Carlo approach to the Glauber model simulates heavy-ion collisions on an event-by-event basis by randomly sampling the positions of individual nucleons within each nucleus according to a given nuclear density distribution, such as the Woods–Saxon profile. For each generated event, the nuclei are shifted by an impact parameter and nucleon–nucleon interactions are determined based on a geometric criterion using the inelastic nucleon–nucleon cross-section.

This method yields key quantities such as the number of participating nucleons (N_{part}), the number of binary collisions (N_{coll}), and spatial anisotropies (e.g., eccentricities) specific to each event. These quantities are essential for characterizing the initial conditions of the collision and serve as inputs for subsequent dynamical modeling.

Chapter 3

The Monte Carlo Glauber Approach

The Glauber Monte Carlo (MC) model has become an indispensable tool in the theoretical and experimental study of relativistic heavy-ion collisions. It provides a geometrical framework for modeling the initial stage of such collisions by simulating the positions and interactions of individual nucleons on an event-by-event basis. This statistical approach allows researchers to connect the underlying collision geometry with a wide range of observables, such as multiplicity distributions, anisotropic flow, and nuclear modification factors Miller et al. (2007*b*).

At the heart of the Glauber MC model is the idea that nucleons within each colliding nucleus can be represented as point-like objects distributed according to a probabilistic nuclear density profile, typically of Woods–Saxon form. In each simulated event, the two nuclei are randomly positioned with a chosen impact parameter, and nucleons are said to collide if their transverse separation is less than a threshold determined by the inelastic nucleon–nucleon cross-section, $\sigma_{NN}^{\text{inel}}$ Miller et al. (2007*a*).

This stochastic procedure generates key geometric quantities for each event, such as the number of participant nucleons (N_{part}), the number of binary collisions (N_{coll}), and the spatial eccentricities (ε_2, ε_3, etc.). These quantities characterize the shape and size of the interaction zone and are crucial for understanding the initial conditions that drive the evolution of the quark-gluon plasma in hydrodynamic models Ray and Daugherity (2007).

Because of its flexibility and event-by-event capability, the Monte Carlo version of the Glauber model has become the standard initial-state model in modern heavy-ion physics. It is employed by major experimental collaborations at RHIC and the LHC to determine collision centrality, estimate geometric fluctuations, and provide input for dynamical simulations. In particular, its role in connecting nuclear geometry to electromagnetic field distributions has gained increasing importance in recent years, especially for the study of phenomena such as the chiral magnetic effect.

3.1 Procedure :

The Monte Carlo Glauber model simulates nucleus–nucleus collisions by generating nucleon configurations and computing geometric properties event-by-event. The general procedure can be broken down into the following key steps:

1. **Sampling Nucleon Positions:**
   The positions of nucleons within each nucleus are sampled randomly from a nuclear density distribution, typically a Woods–Saxon profile:

$$\rho(r) = \frac{\rho_0}{1 + \exp\left(\frac{r-R}{a}\right)}, \tag{3.1}$$

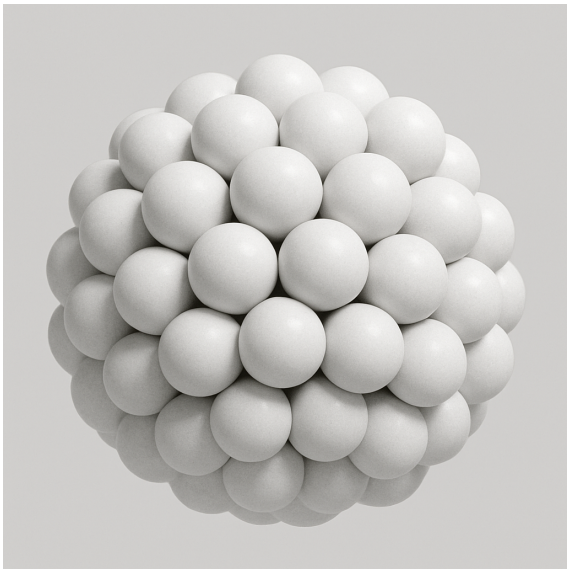

Figure 3.1: First stage of generating nucleus

where R is the nuclear radius, a is the skin depth, and ρ_0 is the central density.

2. **Assigning Impact Parameter:**
   For each collision event, an impact parameter b is randomly selected from a probability distribution proportional to b, i.e., $P(b)\,db \propto b\,db$. This represents the transverse distance between the centers of the two colliding nuclei.

3. **Shifting Nuclei in Impact Plane:**
   The two nuclei are spatially separated in the transverse plane by the sampled impact parameter b, and their nucleons are positioned accordingly.

4. **Determining Binary Collisions:**
   A nucleon–nucleon collision occurs if the transverse distance between a pair of nucleons (one from each nucleus) is less than the interaction range, defined by the inelastic nucleon–nucleon cross-section $\sigma_{NN}^{\text{inel}}$:

$$d \leq \sqrt{\frac{\sigma_{NN}^{\text{inel}}}{\pi}}. \tag{3.2}$$

   All such pairs are counted as binary collisions.

5. **Identifying Participants and Collisions:**
   A nucleon is labeled a *participant* if it undergoes at least one inelastic interaction. The total number of binary collisions (N_{coll}) and participant nucleons (N_{part}) are recorded for each event.

6. **Calculating Event Geometry:**
   Using the positions of participating nucleons, one calculates geometric observables like the eccentricities (ε_2, ε_3), center-of-mass shifts, and transverse overlap area. These are vital for initializing hydrodynamic or electromagnetic field simulations.

7. **Repeating Over Many Events:**
   This process is repeated over a large number of statistically independent events to build up distributions of observables and extract meaningful averages and fluctuations.

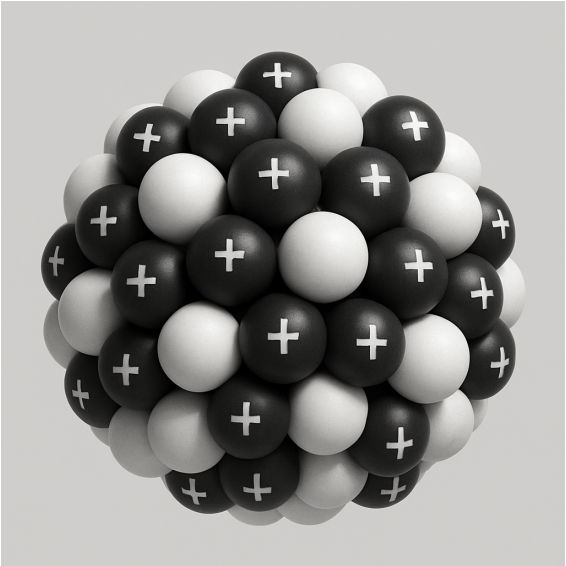

Figure 3.2: Randomly selected protons and neutrons inside a nucleus

This systematic approach allows for the generation of realistic, fluctuating initial conditions in high-energy nuclear collisions, forming a critical input for further dynamical modeling and phenomenological analysis.

3.2 Specifications of the Computer Program:

3.2.1 Nuclear Charge Density :

The standard method employed in high-energy heavy-ion collisions describes the initial transverse shape of the nuclei in terms of 2-parameter Fermi ($2pF$) distributions (also often called Wood-Saxon distribution) with half-density radius (R) & diffusivity parameter (a) obtained from fits to elastic lepton-nucleus data De Jager et al. (1974).

$$\rho(r) = \frac{\rho_0}{1 + \exp\frac{(\rho - R)}{a}} \tag{3.3}$$

where ρ_0 is a normalization constant so that

$$\int_{V \geq V_{atom}} dV \rho(r) = 1 \tag{3.4}$$

where V is volume and V_{atom} is volume of the atom. R describes the mean location of the nucleus area (that is, R is indicative of the extension of the bulk part of the density distribution). The diffusivity parameter a describes the tail of the density profile.

However, neutron-rich nuclei, such as ^{208}Pb can have **differing proton & neutron density distributions** in the nuclear periphery. In fact, measurements have recently been able to extract the neutron profile of several nuclei that show differences with respect to their proton distribution Kłos et al. (2007); Tarbert et al. (2014) & various works have already studied

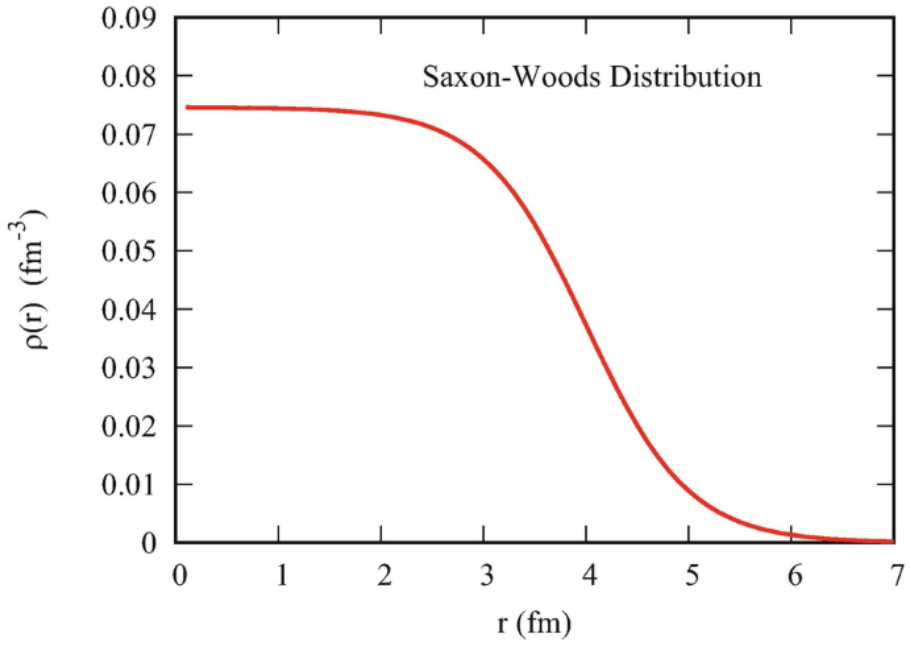

Figure 3.3: $\rho(r)$ vs r plot according to the Wood-Saxon distribution

its impact on different isospin-dependent observables in nuclear collisions Paukkunen (2015); De (2017).

3.2.2 Lienard-Wiechert potentials :

In the relativistic regime, the electromagnetic fields generated by moving point charges must be described using the Liénard–Wiechert potentials. Developed in classical electrodynamics, these potentials yield exact expressions for the scalar and vector potentials Φ and $\mathbf{A}$ from a charge undergoing arbitrary motion at any velocity up to the speed of light Bel and Martín (1973). In particular, the advanced and retarded forms derived by Bel and Martín enable a self-consistent perturbative evaluation of fields in a predictive relativistic framework Bel and Martín (1973).

When applying these potentials to high-energy heavy-ion collisions, one must rigorously account for relativistic effects such as Lorentz contraction and retardation. Deng and Huang (2012) demonstrated an event-by-event implementation of these potentials—coupled with collision event generators like HIJING—to analyze the spatial and temporal distributions of electric and magnetic fields in ultra-relativistic collisions Deng and Huang (2012).

A robust computational implementation—such as that described in Jackson's electrodynamics text—handles:

- **Trajectory input:**
  time-dependent positions and velocities of charged particles (e.g., spectators and participants in a Pb–Pb collision), typically sampled from Monte Carlo Glauber outputs.

- **Field computation:**
  evaluation of electromagnetic fields using the standard Liénard–Wiechert field equations for relativistic limits:

$$\mathbf{E}(t,\mathbf{r}) = \frac{e}{4\pi}\sum_n Z_n \frac{\mathbf{R}_n - R_n\mathbf{v}_n}{(R_n - \mathbf{R}_n\cdot\mathbf{v}_n)^3}(1-v_n^2), \tag{3.5}$$

$$\mathbf{B}(t,\mathbf{r}) = \frac{e}{4\pi}\sum_n Z_n \frac{\mathbf{v}_n \times \mathbf{R}_n}{(R_n - \mathbf{R}_n\cdot\mathbf{v}_n)^3}(1-v_n^2), \tag{3.6}$$

where,

$\mathbf{R}_n = \mathbf{r} - \mathbf{r}_n$ is the vector from the field point $\mathbf{r}$ to the position of the n-th charged particle.

$\mathbf{Z_n}$ is the atomic number (i.e., the electric charge in units of e) of the n-th particle.

$\mathbf{v}_n$ is the velocity vector of the n-th particle.

$v_n = |\mathbf{v}_n|$ is the magnitude of the velocity of the n-th particle.

All quantities are evaluated at the *retarded time*, which satisfies the causality condition: the field at $(t,\mathbf{r})$ depends on the source position at an earlier time t_r such that $t_r = t - |\mathbf{r} - \mathbf{r}_n(t_r)|/c$.

The computational code operates in the ultra-relativistic limit ($\gamma \gg 1$), optimizing field evaluation for programming efficiency and numerical stability, relying on the fundamental Liénard–Wiechert formalism without further approximations.

This subsection outlines the numerical parameters, program structure, and relativistic considerations required for accurate electromagnetic field computation. The implementation forms the basis for later analysis of field evolution and phenomenological implications in Pb–Pb collisions at LHC energies.

Chapter 4

Results And Discussions

This section presents the quantitative results obtained from the simulation of electromagnetic field generation in ultra-relativistic Pb–Pb collisions using the Monte Carlo Glauber model framework. The spatial and temporal profiles of the electric and magnetic fields were computed event-by-event based on nucleon distributions sampled according to the Woods–Saxon density function. The electromagnetic fields were evaluated using the relativistic Liénard–Wiechert potential formalism, incorporating contributions from both participant and spectator nucleons.

The following graphs and visualizations illustrate the evolution of various components of the electric and magnetic fields as functions of time, spatial coordinates, and collision centrality. Special emphasis is placed on the transverse magnetic field (B_y), the longitudinal electric field (E_z), and their correlation with geometric quantities such as impact parameter and nucleon configuration. These results highlight the magnitude, orientation, and event-by-event fluctuations of the fields, offering deeper insight into their physical relevance in the context of high-energy nuclear collisions.

4.1 Generation of Nucleons

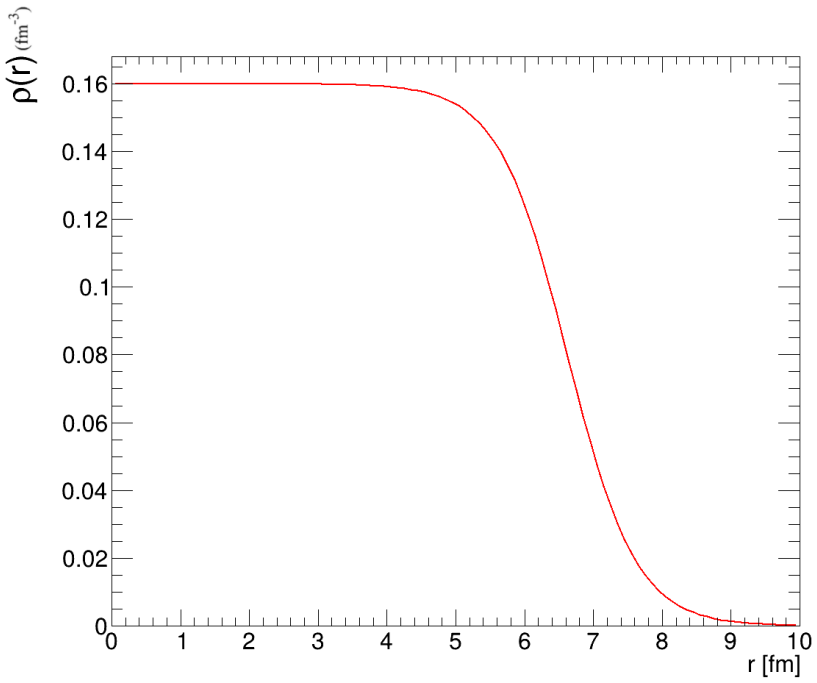

Figure 4.1: Wood-Saxon distribution plot from our calculation

The plot above represents the Wood-Saxon nuclear density distribution generated from the simulation code implemented as part of this project. The distribution accurately captures the expected nuclear density profile, characterized by a near-constant density in the central region of the nucleus and a gradual fall-off near the nuclear surface. The output is consistent with the theoretical form of the Wood-Saxon distribution, validating the correctness of the implemented algorithm and parameter choices. This agreement also confirms that the spatial configuration of nucleons used in the MC Glauber simulations closely reflects realistic nuclear geometry.

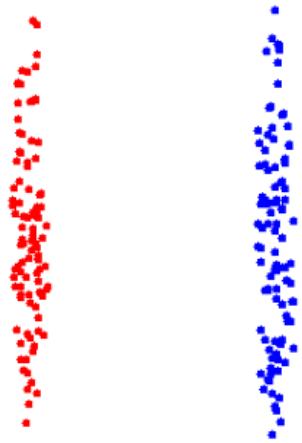

Figure 4.2: Randomly generated nucleons moving at relativistic speed at t=0

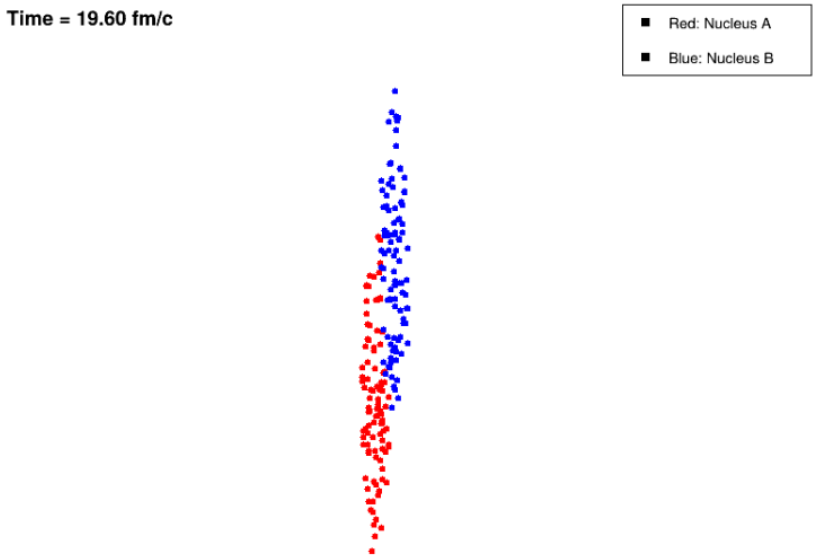

Figure 4.3: Collision of nuclei at relativistic speed at $t = 19.60 f\,mc^{-1}$

One of the key visualizations in our results demonstrates the effect of Lorentz contraction on the shape of the nucleus during ultra-relativistic motion. The nucleons are moving along x-direction. As the heavy nuclei approach each other at velocities close to the speed of light, the individual nucleons experience a significant flattening along the direction of motion due to relativistic effects. This results in an ellipsoidal (pancake-like) geometry when viewed in the laboratory frame. The figure above captures this deformation, where the spherical symmetry of the rest-frame nucleons is altered into an oblate shape along the beam axis. This Lorentz-contracted geometry plays a crucial role in determining the spatial overlap region, influencing initial state anisotropies and, consequently, the resulting electromagnetic field distributions and collective flow phenomena in the collision.

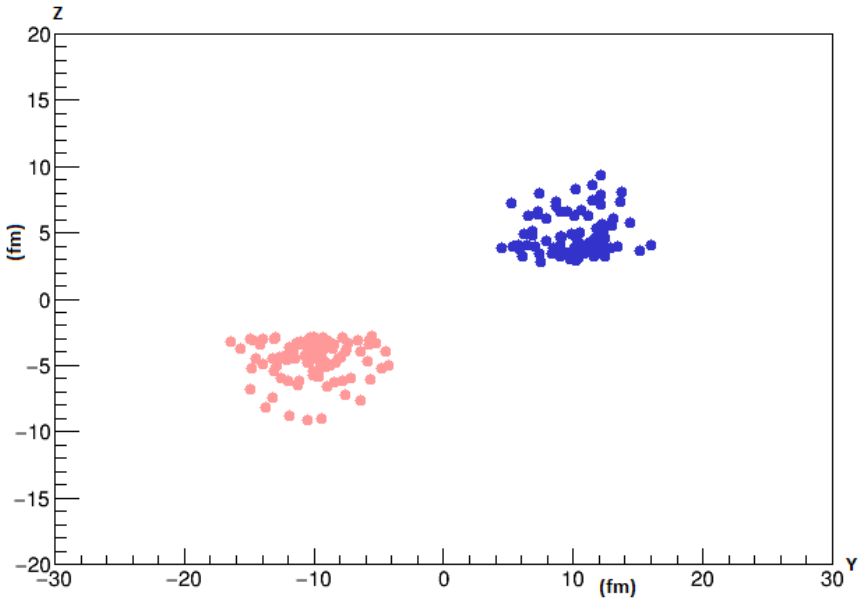

Figure 4.4: Spectators after the collision in transverse plane

4.2 EMF-field Components :

4.2.1 Electric Field vs Impact Parameter

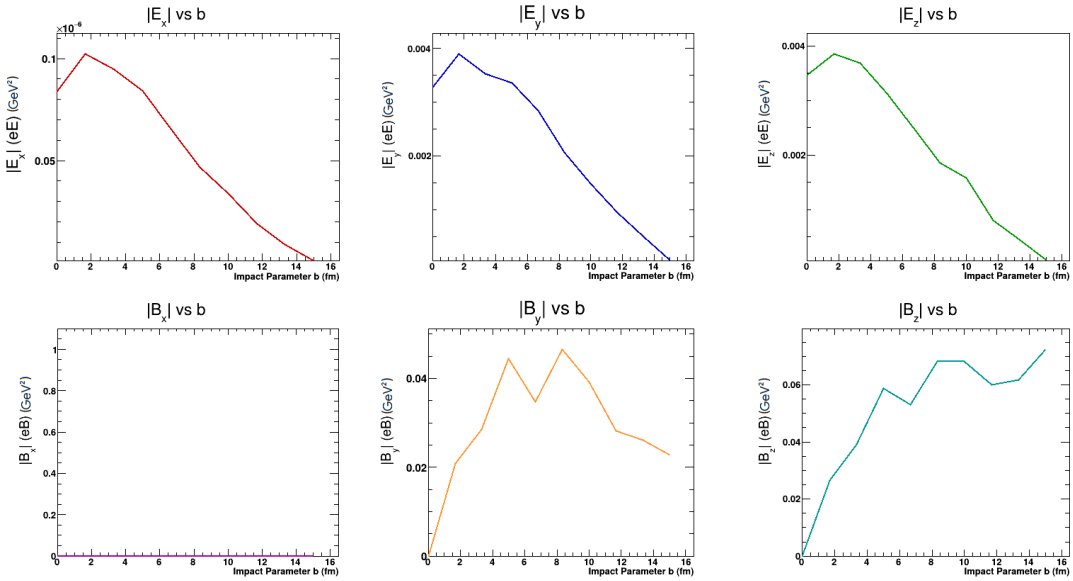

Figure 4.5: Event – by – event variation of electric field (up) and magnetic field (down) with impact parameter for Pb + Pb collision at center-of-mass energy 2760GeV moving along X-axis

- **Key Findings of The Electric Field:**
  - The electric field at b=0 is nonzero and has a value which are $|E_x| \in (0.08, 0.09)$, $|E_y| \in (0.08, 0.09)$ and $E_z$is nearly equal to 0.0035.

- Then the electric field value increases monotonically to the peak value at $b \in (1.5, 2.0)$.
- Later the value of the electric field decreases monotonically after reaching the maximum value.
- The value of the electric field is zero at b=15 fm

- **Key Findings of The Magnetic Field :**
  - The magnetic field value for b=0 is zero.
  - It is constantly equals to zero along all values of impact parameter for $|B_x|$, because the movement of ions are along x-axis.
  - It increases monotonically to a crest value $|B_y| \approx 0.045$ in $b \approx 5fm$. Then it decreses linearly to an extent $|B_y| \approx 0.035$ and then increases to a peak value $|B_y| \in (0.045, 0.05)$ at $b \in (8.0, 8.5)$. And finally decreases monotonically to $|B_y| \in (0.02, 0.025)$ at $b \approx 15fm$.
  - The value of magnetic field increases monotonically to a crest $|B_z| \in (0.055, 0.06]$ at $b \approx 5fm$. Then it decreases to an extent $|B_z \in (0.05, 0.055)$ at $b \in [6.5, 7.0)$ then increase monotonically for a creast value.
  - It remains constant for an extent at $|B_z| \in (0.065, 0.07)$ for $b \approx 10fm$. Later the magnetic field decreases and increases monotonically to $|B_z| \in (0.07, 0.075)$ at $b \approx 15fm$.

4.2.2 Magnetic field vs Time :

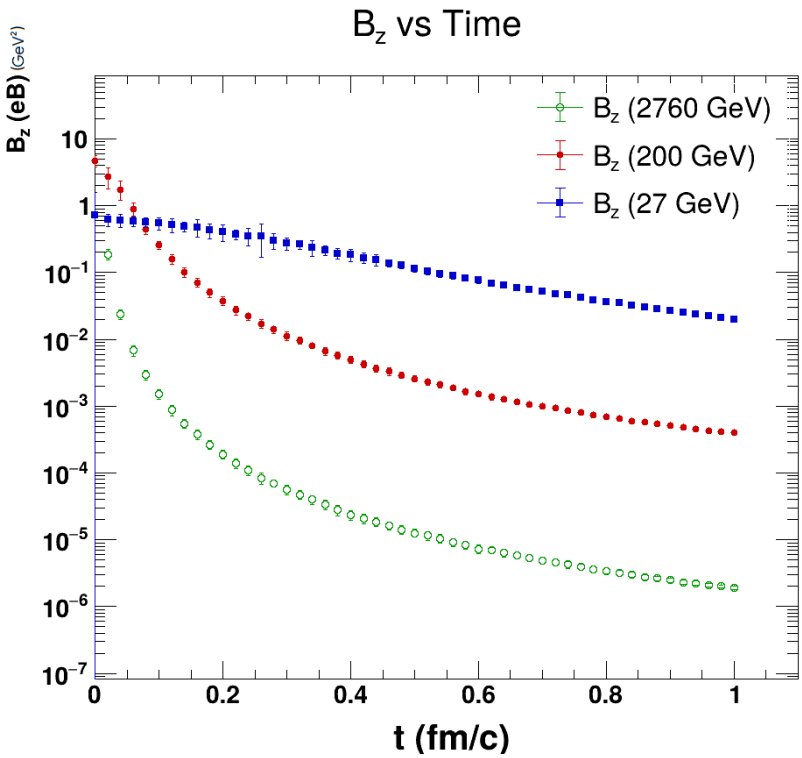

Figure 4.6: Time evolution of magnetic field at LHC and RHIC energies

- **Key Findings of Time Evolution of Magnetic Field :**

- The value of magnetic fields for all collision energies is highest at $t = 0fmc^{-1}$.
- During the evolution magnetic field decreases.
- Magnetic fields from higher-energy collisions decrease rapidly than the one at low energy.
- It decreases exponentially for LHC energy and RHIC energy = 200GeV while it decreases very slowly for RHIC energy = 27GeV.

Chapter 5

Conclusions and Future Work

5.1 Conclusion

- We have simulated the nucleon distribution with nucleus for Au and Pb ions using Wood-Saxon potential.
- We let them move with **relativistic velocity**. A moving electric charge constitutes an electric current, which in turn gives rise to a magnetic field. We simulated **the time and space distribution of the electric field and magnetic field** at energies $2.76\,TeV$, $200GeV$ and $27GeV$.
- We observe a very strong and transient EM field. The typical magnitude of magnetic field at one of the top LHC energies from our calculation is $0.05GeV^2$. In natural units $1GeV^2$ is $\approx 10^{20}Gauss$. therefore, from our calculation magnitude of magnetic field comes to be of the order of $10^{18}Gauss$, **much stronger than the magnetic field of Earth (**$0.5Gauss$**)**.

5.2 Future Work

Several extensions of this work can be pursued in the future:

- These calculations can be extended to determine the strength of synchrotron radiation
- Studying the influence of these fields on charged particle flow and quark-gluon plasma (QGP) dynamics.
- Exploring similar calculations for asymmetric systems such as p–Pb and Cu–Au collisions.

These developments would further enhance the understanding of initial-state effects and electromagnetic phenomena in relativistic heavy-ion collisions.

References

Anonymous (2020), 'Collision-geometry-based 3d initial condition for relativistic heavy-ion collisions', *Phys. Rev. C* **102**. Defines the impact vector as pointing from target to projectile centers.

B. Muller, J. S. and Wyslouch, B. (2012), 'First results from pb+pb collisions at the lhc', *Ann. Rev. Nucl. Part. Sci.* **62**, 361–386.

Bel, L. and Martín, J. (1973), 'Approximate solutions of predictive relativistic mechanics for the electromagnetic interaction. ii', *Phys. Rev. D* **8**, 4347.

Cugnon, J. (1980), 'Monte carlo simulation of nucleus–nucleus collisions', *Physical Review C* **22**(5), 1885.

D. E. Kharzeev, J. Liao, S. A. V. G. W. (2016), 'Chiral magnetic and vortical effects in high-energy nuclear collisions—a status report', *Prog. Part. Nucl. Phys.* **88**, 1–28.

D. Teaney, J. L. and Shuryak, E. V. (2001), 'Flow at the sps and rhic as a quark-gluon plasma signature', *Phys. Rev. Lett.* **86**, 4783.

De Jager, C., De Vries, H. and De Vries, C. (1974), 'Nuclear charge- and magnetization-density-distribution parameters from elastic electron scattering', *Atomic Data and Nuclear Data Tables* **14**(5), 479–508. Nuclear Charge and Moment Distributions.
URL: *https://www.sciencedirect.com/science/article/pii/S0092640X74800021*

De, S. (2017), 'The effect of neutron skin on inclusive prompt photon production in Pb + Pb collisions at Large Hadron Collider energies', *J. Phys. G* **44**(4), 045104.

Deng, W.-T. and Huang, X.-G. (2012), 'Event-by-event generation of electromagnetic fields in heavy-ion collisions', *Phys. Rev. C* **85**, 044907.

d'Enterria, D. (2003), 'Hard scattering cross sections at lhc in the glauber approach: from pp to pa and aa collisions', *arXiv:nucl-ex/0302016* .

Esha, R. T. (2012), Glauber modeling of high energy heavy ion collision.
URL: *https://api.semanticscholar.org/CorpusID:210151810*

et al., M. L. M. (2007), 'Glauber modeling in high-energy nuclear collisions', *Annu. Rev. Nucl. Part. Sci.* **57**, 205–243.

et al., V. V. (2014), 'Time dependence of partition into spectators and participants in relativistic heavy-ion collisions', *arXiv:1407.4644* .

Gelis, F. (2013), 'Color glass condensate and glasma', *Prog. Part. Nucl. Phys.* **70**, 63–87.

Glauber, R. J., Miller, M. L., Alver, B., Adams, J., Back, B. B. and Daugherity, M. (2008), 'Glauber modeling in high energy nuclear collisions', *Journal of Physics G: Nuclear and Particle Physics* **35**(12), 125106.

Heinz, U. and Jacob, M. (2000), 'Evidence for a new state of matter: An assessment of the results from the cern lead beam programme', *arXiv:nucl-th/0002042* .

Hirano, T. and Nara, Y. (2013), 'Integrated dynamical approach to relativistic heavy-ion collisions', *Prog. Part. Nucl. Phys.* **70**, 108–158.

Kłos, B., Trzcińska, A., Jastrzębski, J., Czosnyka, T., Kisieliński, M., Lubiński, P., Napiorkowski, P., Pieńkowski, L., Hartmann, F. J., Ketzer, B., Ring, P., Schmidt, R., Egidy, T. v., Smolańczuk, R., Wycech, S., Gulda, K., Kurcewicz, W., Widmann, E. and Brown, B. A. (2007), 'Neutron density distributions from antiprotonic ^{208}Pb and ^{209}Bi atoms', *Phys. Rev. C* **76**, 014311.
URL: *https://link.aps.org/doi/10.1103/PhysRevC.76.014311*

Lectures on high-energy heavy-ion collisions at the LHC (2009), Technical report, CERN. See page 5: "The impact parameter which is the distance between the centres of the two colliding nuclei. . . ".

Loizides, C., Kamin, J. and d'Enterria, D. (2018), 'Improved monte carlo glauber predictions at present and future nuclear colliders', *Phys. Rev. C* **97**(5), 054910.

Loizides, C., Kamin, J. and d'Enterria, D. (2019), 'Erratum: Improved monte carlo glauber predictions at present and future nuclear colliders', *Phys. Rev. C* **99**(1), 019901.

Miller, M. L., Reygers, K., Sanders, S. J. and Steinberg, P. (2007*a*), 'Glauber modeling in high energy nuclear collisions', *arXiv:nucl-ex/0701025* .

Miller, M. L., Reygers, K., Sanders, S. J. and Steinberg, P. (2007*b*), 'Glauber modeling in high-energy nuclear collisions', *Annu. Rev. Nucl. Part. Sci.* **57**, 205–243.

Participants and spectators at the heavy-ion fireball (2012), *CERN Courier* .

Paukkunen, H. (2015), 'Neutron skin and centrality classification in high-energy heavy-ion collisions at the LHC', *Phys. Lett. B* **745**, 73–78.

Ray, R. L. and Daugherity, M. (2007), 'Applicability of monte carlo glauber models to relativistic heavy ion collision data', *arXiv:nucl-ex/0702039* .

ROOT Collaboration (2025), 'Histograms tutorial examples (TH1/TH2)', https://root.cern/doc/v636/group__tutorial__hist.html#th2. Thorough examples for 1-D and 2-D histograms in ROOT.

Segal, I. and Taranenko, A. (2023), 'The impact of the fragmentation processes of spectators on the centrality determination in heavy-ion collisions', *J. Phys.: Conf. Ser.* .

Song, H. and Heinz, U. (2011), 'Extracting the qgp viscosity from rhic data – a status report from viscous hydrodynamics', *J. Phys. G* **38**, 124151.

Stephanov, M. A. (2004), 'Qcd phase diagram and the critical point', *Prog. Theor. Phys. Suppl.* **153**, 139–156.

Tarbert, C. M. et al. (2014), 'Neutron skin of ^{208}Pb from Coherent Pion Photoproduction', *Phys. Rev. Lett.* **112**(24), 242502.

Tejeda-Yeomans, M. (2020), 'Heavy-ion physics: freedom to do hot, dense, exciting qcd'.

Wang, L., Xu, Y. and Chen, Z. (2024), 'Study of eccentricities in lead–lead collisions using glauber model', *Proceedings of the 4th International Conference on High Energy Physics and Applications* **43**.

Wang, Z., Zhang, J. and Li, B. (2021), Monte carlo glauber modeling of pb–pb collisions at lhc, *in* 'Frontiers in Science and Smart Technology', pp. 123–128.

Appendix A

Differences And Similarities Between Optical and Monte Carlo Glauber Model

A.1 Differences

Table A.1: Comparison of Optical and Monte Carlo Glauber Models

Aspect	**Optical Glauber Model**	**Monte Carlo Glauber Model**
Nuclear Density	Treated as a continuous, smooth density function (e.g., Woods–Saxon profile)	Nucleons are sampled individually from the same density distribution
Event Treatment	Provides averaged results over many hypothetical collisions	Simulates each collision event explicitly, allowing for fluctuations
Participants and Collisions	N_{part} and N_{coll} are calculated through integrals over continuous thickness functions	Determined by counting discrete nucleon–nucleon interactions in each event
Fluctuations	Does not include event-by-event fluctuations	Naturally incorporates fluctuations in nucleon positions and geometry
Computational Speed	Faster and analytically tractable	Slower due to the need to simulate many events
Use Cases	Suitable for quick, average estimates or theoretical modeling	Preferred for realistic simulations in experimental analyses
Centrality Determination	Gives average quantities per centrality class	Enables mapping of observables to centrality on an event-by-event basis
Eccentricity Calculation	Yields smooth eccentricity profiles	Captures higher-order eccentricities and their fluctuations (ε_2, ε_3, etc.)
Geometry Resolution	Limited to smooth nuclear overlap	Resolves fine-scale spatial structure of initial geometry

A.2 Similarities

Despite methodological differences, the Optical and Monte Carlo versions of the Glauber model share several core principles and applications. These similarities include:

- **Common Theoretical Framework:**
  Both approaches are based on the same geometric Glauber formalism, designed to model high-energy nucleus–nucleus collisions and compute observables such as the impact parameter (b), the number of participating nucleons (N_{part}), and the number of binary collisions (N_{coll}) Miller et al. (2007*b*).

- **Use of Identical Nuclear Density Profiles:**
  Both models use the same nuclear density functions, typically the Woods–Saxon distribution, to sample or describe the spatial distribution of nucleons inside the colliding nuclei Miller et al. (2007*a*).

- **Straight-line Trajectories (Eikonal Approximation):**
  In both models, nucleons are assumed to travel in straight-line paths along the beam axis. The effect of scattering or deflection is neglected, which is valid at ultra-relativistic energies Miller et al. (2007*b*).

- **Fixed Inelastic Cross-section:**
  The inelastic nucleon–nucleon cross-section ($\sigma_{NN}^{\text{inel}}$) is taken as a constant input in both models and is used to determine whether two nucleons interact during a collision event Miller et al. (2007*a*).

- **Agreement in Average Observables:**
  For large collision systems and mid-central events, both models yield similar average values of N_{part}, N_{coll}, and total inelastic cross-section, reinforcing their physical consistency Miller et al. (2007*b*).

- **Centrality Determination:**
  Both models are extensively used to define centrality classes in experimental heavy-ion collision analyses, allowing mapping of collision observables to geometry-based quantification Miller et al. (2007*b*).

- **Initial Conditions for Further Modeling:**
  Outputs from both models—such as geometry, participant distributions, and impact parameters—serve as standard inputs to further dynamical models including hydrodynamics, parton transport, and electromagnetic field simulations Miller et al. (2007*a*).

Appendix B

ROOT Histogram Tutorials

The following table summarizes ROOT tutorials for creating and working with 1-D and 2-D histograms (TH1, TH2), as referenced from the official ROOT documentation ROOT Collaboration (2025). These examples guided my implementation of histogram-based data visualization.

Tutorial File (Link)	Histogram Type	Description
h1draw.C	1-D (TH1)	Demonstrates creation, filling, and drawing of a 1-D histogram using random data. :contentReference[oaicite:1]index=1
h2proj.C	2-D (TH2)	Shows how to project a 2-D histogram onto 1-D axes; illustrates projections along X and Y. :contentReference[oaicite:2]index=2
TH2 Class Reference	2-D (TH2)	Provides comprehensive reference for all TH2 methods, including Fill, Projection, and styling—useful for building custom 2-D histogram workflows. :contentReference[oaicite:3]index=3
THistPainter Class Reference	1-D/2-D Drawing	Details available drawing options (e.g., "lego", "contour") and usage of Draw() method for histograms. :contentReference[oaicite:4]index=4

Table B.1: Selected ROOT histogram tutorials and reference guides with links and descriptions.